

HYDRODYNAMICAL SIMULATION OF THE STRUCTURE OF THE X-RAY PULSAR ACCRETION CHANNEL: ACCOUNTING FOR RESONANT SCATTERING

I. D. Markozov^{1*}, A. D. Kaminker¹, A. Y. Potekhin¹

¹*Ioffe Institute, Politekhnikeskaya 26, St. Petersburg, 194021 Russia*

A self-consistent radiation-hydrodynamics model of an accretion channel of subcritical X-ray pulsars is constructed. The influence of the presence of resonance in the scattering cross-section on the accretion process and radiation transfer is taken into account. It is shown that the efficiency of plasma deceleration by radiation depends on the magnitude of the magnetic field B . For $B = 1.7 \times 10^{12}$ G, the spectra and the degree of linear polarization of the radiation of the accretion channel are constructed. In the obtained spectra, the shape of the cyclotron line depends on the direction of the outgoing radiation. The calculated linear polarization degree of the outgoing radiation is 30 – 40% near the cyclotron resonance, whereas it can be small ($\lesssim 5 - 10\%$) at energies significantly lower than the resonant one.

Keywords: neutron stars, X-ray astronomy.

1. INTRODUCTION

Accreting X-ray pulsars have magnetic fields $10^{11} - 10^{13}$ G (see, e.g., the review by Mushtukov and Tsygankov, 2023). When the plasma moving to such a pulsar reaches the magnetosphere, it freezes into the magnetic field and moves along it to the magnetic poles of the neutron star. The plasma in the accretion channel near the poles moves with moderately relativistic velocities almost perpendicular to the surface (Davidson, 1973). The kinetic energy of the plasma is converted into radiation, whose pressure can be so strong that it affects the dynamics of the infalling matter. The higher the accretion rate, the higher the luminosity. If a certain threshold accretion rate is exceeded, the radiation can completely halt the matter. In this case, a radiation-dominated shock wave is expected to appear in the channel (Basko and Sunyaev, 1976), behind the front of which a region of slow sedimentation of matter is formed. Hereafter, X-ray pulsars of this type will be called *supercritical*, while those with an accretion rate below the threshold will be called *subcritical*.

A large amount of the latest observational data on X-ray pulsars leads to the importance and relevance of theoretical modeling of the structure and radiation of these objects. Meanwhile, currently there is no sufficiently complete theoretical model capable of describing all the variety of physical processes in a wide range of parameters of the X-ray pulsars. Since the radiation generated by accretion actively affects the accretion process itself, theoretical modeling of the structure of the accretion channel and the characteristics of its radiation should be carried out in a self-consistent manner. An example of such calculations in the stationary case has been presented by West et al. (2017a,b). Nonstationary modeling without calculation of spectra was first performed by Klein and Arons (1989). They have demonstrated the formation of a radiation-dominated shock wave in the accretion channel of a supercritical pulsar. A one-dimensional calculation of the process of establishing a stationary flow in the accretion columns of supercritical pulsars was carried out by Abolmasov and Lipunova (2023), who have taken into account the possibility of the column leakage at highly supercritical accretion rates and found the limits of applicability of the ana-

*E-mail: markozoviv@mail.ru

lytical solution of Basko and Sunyaev (1976). The simulations of X-ray pulsar radiation with an accurate account of the magnetic field effect on radiative transfer in the plasma were carried out separately from the solution of the equations of hydrodynamics. The most detailed calculations to obtain the spectra of X-ray pulsars with cyclotron features were performed using the Monte Carlo method by Schwarm et al. (2017).

In this paper, we consider subcritical X-ray pulsars with an accretion channel completely filled with plasma. For such systems, we present the results of self-consistent radiation-hydrodynamical modeling of the channel structure and the its outgoing radiation. An important difference between our work and the previous ones is the joint calculation of radiative transfer and accretion hydrodynamics, taking into account birefringence and resonance scattering in a magnetic field. In addition, the method we use does not employ the diffusion approximation, which allows us to consider subcritical pulsars with low density of matter in accretion channels.

2. MAGNETIC FIELD EFFECTS

Quantization of electron motion across magnetic field lines (e.g., Sokolov and Ternov, 1986) can be important in the accretion channels of the X-ray pulsars. Electrons occupy energy levels (Landau levels), each of which corresponds to a certain value of the transverse momentum. In this case, the total energy of the electron with a momentum along the field p_z at the n th Landau level ($n = 0, 1, 2, \dots$) equals

$$E_n = \sqrt{m^2 c^4 + c^2 p_z^2 + 2nmc^2 E_{\text{cyc}}}, \quad (1)$$

where $E_{\text{cyc}} = \hbar e B / (mc)$ is the cyclotron energy, e is the electron charge, m is its mass, B is the magnetic field strength, \hbar is the reduced Planck constant, and c is the speed of light. We assume that all electrons occupy the ground Landau level, and consider transitions only from the ground level to the ground level, which is justified by the short lifetime of electrons at excited Landau levels compared to the characteristic free path time of an electron in the pulsar magnetosphere (e.g., Mészáros, 1992).

The magnetized plasma is a birefringent medium: the radiation splits in it into two waves, extraordinary and ordinary ones (e.g., Ginzburg, 1970; Gnedin and Pavlov, 1974), which are often called the X-mode and the O-mode. In general, they have

elliptical polarization; the major semiaxis of the ellipse that is the locus of the endpoints of the electric vector of the O-mode lies in the plane formed by the magnetic field vector and the photon wave vector, while the major semiaxis of the ellipse corresponding to the X-mode is perpendicular to this plane.

The ellipticity of normal modes depends on the photon energy and propagation direction. In this paper, it is calculated without allowance for vacuum polarization and temperature effects in the plasma (see, for example, fig. 1 and eq. (3) in Mushtukov et al., 2022). In this case, for the applicability of the normal mode approximation it is sufficient that $\min(\omega, \omega_{\text{cyc}}) \gg \nu_e$ (Gnedin and Pavlov, 1974), where ω is the photon frequency, ω_{cyc} is the electron cyclotron frequency, and ν_e is the collision frequency. The frequencies of radiative and non-radiative collisions of electrons with protons in quantizing magnetic fields are given in the article by Potekhin and Lai (2007). Using them, it is easy to verify that the condition for the applicability of the normal mode approximation in the accretion channel under consideration is fulfilled with a large margin. For example, neglecting Coulomb logarithms for order-of-magnitude estimates and setting $B = 2 \times 10^{12}$ G, $\rho = 10^{-5}$ g/cm³, and $E = T = 1$ keV, we obtain $\nu_e / \omega \sim 10^{-10}$.

The cross sections of radiation processes in a strong magnetic field depend on polarization. In addition, they have resonances, which cause the appearance of cyclotron lines in the X-ray pulsar spectra. We will consider only the processes of Compton scattering of photons by electrons in a strong magnetic field. In this case, the laws of conservation of energy and longitudinal momentum are fulfilled, while the transverse momentum is not conserved. For photons of the normal modes, we use approximate expressions for scattering cross sections obtained by Herold (1979), which contain only the main resonance at the cyclotron energy E_{cyc} . To calculate birefringence, we use the cold plasma approximation (see Ginzburg, 1970; Gnedin and Sunyaev, 1974), which does not take into account the electron thermal motion effect on the dielectric tensor. We also neglect the vacuum polarization (Pavlov and Gnedin, 1984). Full expressions for scattering cross sections in the representation of elliptic modes can be found in the paper by Mushtukov et al. (2022). When averaging cross sections over an ensemble of electrons, we used the relativistic Maxwell distribution with a temperature of $T = 5$ keV. Such an approach, in which T is not cal-

culated in a self-consistent manner, gives only qualitative results for radiation energies in the resonance region.

3. STATEMENT OF THE PROBLEM

We describe plasma motion in the accretion channel by non-relativistic equations of radiation hydrodynamics (see Castor, 2004),

$$\begin{cases} \frac{\partial \rho}{\partial t} + \nabla \cdot (\rho \mathbf{v}) = 0, \\ \frac{\partial \rho \mathbf{v}}{\partial t} + \nabla \cdot (\rho \mathbf{v} \otimes \mathbf{v}) + \nabla p = \mathbf{F}_g + \mathbf{F}_r, \\ \frac{\partial}{\partial t} (\rho \epsilon + \frac{1}{2} \rho v^2) + \nabla \cdot (\rho \mathbf{v} h + \frac{1}{2} \rho \mathbf{v} v^2) = Q_g + Q_r. \end{cases} \quad (2)$$

Here, ρ is the mass density, \mathbf{v} is the plasma velocity, p is the pressure, $\rho \epsilon$ is the internal energy density, and ρh is the enthalpy density of matter; $\mathbf{F}_g = \rho \mathbf{g}$ is the gravitational force density, $Q_g = \rho \mathbf{v} \cdot \mathbf{g}$ is its power, and \mathbf{g} is the gravitational acceleration. We neglect the General Relativity effects, hence $g = GM/r^2$, where M is the mass of the star, r is the distance to its center, and G is the Newtonian constant of gravitation. The term $Q_r = -\int dE \int d\Omega (\epsilon_E - \alpha_E I_E)$ is the power density of energy exchange between the plasma and radiation, $\mathbf{F}_r = -\frac{1}{c} \int dE \int d\Omega \mathbf{\Omega} (\epsilon_E - \alpha_E I_E)$ characterizes their momentum exchange, where α_E is the absorption coefficient of photons with energy E , ϵ_E is their emission coefficient in the medium, $\mathbf{\Omega}$ is a unit vector of photon propagation direction, $d\Omega$ is a solid angle element, and I_E is the specific intensity¹. To calculate I_E , Q_r , and \mathbf{F}_r , one needs to solve the equation of radiative transfer in the medium,

$$\begin{aligned} \mathbf{\Omega} \cdot \nabla I_E^m &= \epsilon_E^m - \alpha_E^m I_E^m \\ &= \sum_{q=1}^2 \int_0^\infty dE' \int_{4\pi} d\Omega' [R_{mq}(E, \mathbf{\Omega}|E', \mathbf{\Omega}') I_{E'}^q(\mathbf{\Omega}') \\ &\quad - R_{qm}(E', \mathbf{\Omega}'|E, \mathbf{\Omega}) I_E^m(\mathbf{\Omega})]. \end{aligned} \quad (3)$$

Here, subscripts m and q denote photon polarization ($m, q = 1$ and 2 for the X- and O-mode, respectively), $R_{mq}(E, \mathbf{\Omega}|E', \mathbf{\Omega}')$ is the scattering coefficient for photons with energy E' , which move in the direction $\mathbf{\Omega}'$ and have polarization q , into the

state with energy E , direction $\mathbf{\Omega}$, and polarization m . We neglect true absorption and emission, as well as stimulated processes, and consider only scattering in which the photon is preserved. The total specific intensity and the total emission coefficient are given by the sum of the polarizations: $I_E = \sum_{m=1}^2 I_E^m$, $\epsilon_E = \sum_{m=1}^2 \epsilon_E^m$.

One needs to set boundary conditions to the system of radiation hydrodynamics equations (2). We assume that the matter at the upper boundary of the channel is in the free-fall state and at a certain fixed accretion rate \dot{M} its velocity is $v = \sqrt{\frac{2GM}{R+H}}$, where R is the neutron-star radius and H is the height of the channel. We neglect the gas pressure at the upper boundary. It does not significantly affect the resulting solutions, since the flow dynamics weakly depends on the gas pressure.

The problem of choosing boundary conditions at the neutron-star surface is less trivial. This problem was discussed, for example, in the works by Basko and Sunyaev (1976) and Kirk (1984). Here we choose the simplest type of boundary condition: $\dot{E}_r = \dot{E}_k + \dot{E}_{\text{back}}$, where \dot{E}_k is the kinetic energy of matter flowing into the lower boundary per unit time, \dot{E}_{back} is the power of radiation scattered from the accretion channel to the lower boundary, and \dot{E}_r is the power of radiation emitted from the lower boundary and having a Planck spectrum. It is also assumed that all matter is in the free-fall state at the initial moment of time.

4. METHOD OF SOLUTION

The joint system of equations of radiation hydrodynamics and radiation transfer was solved using a splitting scheme. The time step was divided into two substeps. At the first substep, the hydrodynamic equations were solved without radiation. This was done using the VH-1 library (“Virginia Hydrodynamics 1”, <http://wonka.physics.ncsu.edu/pub/VH-1>). It implements a piecewise parabolic method of the third order of accuracy with a transition to a Lagrangian grid (PPMLR, developed by Colella and Woodward, 1984), which belongs to the class of Godunov methods. At the second substep the Monte Carlo method was used to calculate the radiation transfer. The distributions obtained at the first substep were used as the values of density and velocity in the accretion channel at the second substep. During the elementary scattering process,

¹Quantities I_E and ϵ_E are normalized to the unit photon energy interval: $I_E = I_\nu/(2\pi\hbar)$, $\epsilon_E = \epsilon_\nu/(2\pi\hbar)$, where I_ν and ϵ_ν are the specific intensity and emission coefficient, normalized to the unit frequency interval (e.g., Sobolev, 1969).

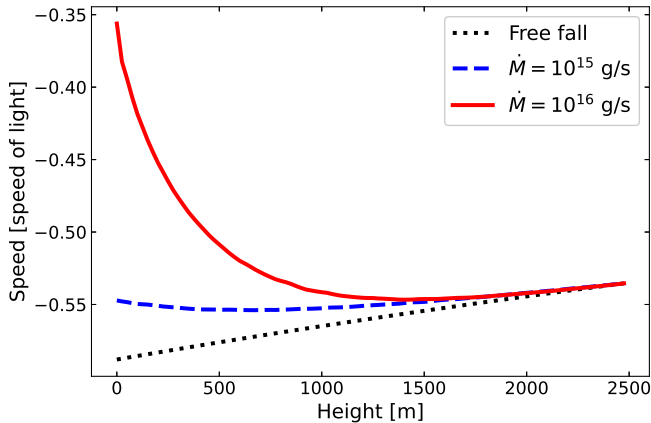


Fig. 1. Accreting matter velocity profiles in units of the speed of light as functions of the height above the neutron-star surface. The black dotted line corresponds to free fall, the blue dashed line corresponds to the accretion rate $\dot{M} = 10^{15}$ g/s, and the red solid line corresponds to $\dot{M} = 10^{16}$ g/s. The parameters are $M = 1.4M_{\odot}$, $R = 12$ km, $R_c = 1$ km, $H = 2.5$ km; the Thomson scattering cross section is used. All values are averaged along the radial coordinate in the accretion channel and correspond to steady-state currents.

the change in plasma energy and momentum at a given point was calculated. Further, according to the known changes in these values for the entire radiation substep, the final values of plasma pressure and velocity were recalculated.

To account for Compton scattering, we generated tables of the cumulative distribution function $f_{mq}(E_i, \theta_i, \theta_f)$ for the probability that a photon with energy E_i and polarization q , initially moving at angle θ_i , to the magnetic field will get polarization m and angle θ_f to the magnetic field after scattering. The tabular values f were interpolated for arbitrary parameter values in the rest frame of scattering electrons. The accreting matter moves at a certain speed, so first a transition is made from the reference frame of the neutron star to the (moving) rest frame of the plasma. Photon energy E_i^p and angle θ_i^p are calculated in the latter reference frame according to the formulae of the Lorentz transformation. The value of the angle after scattering in the plasma reference frame is obtained as $\theta_f^p = f^{-1}(E_i^p, \theta_i^p, \eta)$, where η is a generated random value with uniform distribution and f^{-1} is the inverse function. The angle in the reference frame of a neutron star is obtained using the inverse Lorentz transformations. The photon energy after scattering at a known angle is calculated according to the laws of energy and momentum conservation (where, in the considered case

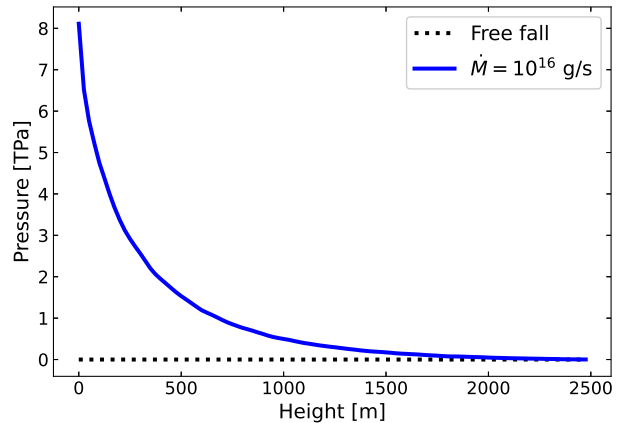


Fig. 2. Pressure profiles in the accretion channel (in units of 10^{12} Pa), averaged along the radial coordinate (of the cylinder), as functions of height above the neutron-star surface. The black dotted line corresponds to free fall and the solid blue one to the steady flow with accretion rate $\dot{M} = 10^{16}$ g/s.

of $n = 0$, it is sufficient to take into account only the longitudinal momentum of the electron, p_z).

We neglect the curvature of the magnetic field and assume that the accretion channel has the shape of a cylinder. This approximation is justified when the heights at which the radiation pressure affects the plasma dynamics are small compared to the radius of a neutron star. The channel was divided into slices of equal height, and in the transverse coordinate (the radius measured from the axis of the cylinder) it was divided into rings of equal areas. We assume that the plasma is completely frozen in a magnetic field. Then there is no macroscopic motion of matter across the field lines, and the two-dimensional hydrodynamic problem turns into a series of one-dimensional ones: a separate calculation is performed for each ring. On the contrary, the radiation transfer was calculated in the completely three-dimensional form.

5. NUMERICAL SIMULATION RESULTS

The main parameters of the model are the mass of the neutron star M , its radius R , the accretion rate \dot{M} , the radius of the accretion channel R_c , its height H , and the cyclotron energy E_{cyc} . We considered a neutron star with mass $M = 1.4M_{\odot}$ and radius $R = 12$ km and an accretion channel with radius $R_c = 1$ km and height $H = 2.5$ km.

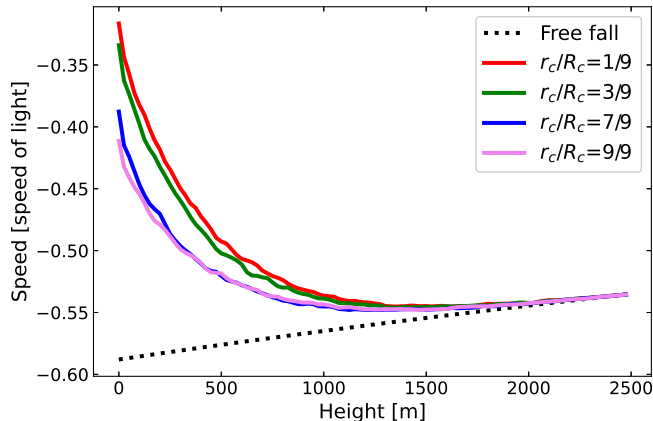


Fig. 3. Velocity profiles of matter in units of the speed of light as functions of height above the neutron-star surface at different distances r_c from the axis of the accretion channel. The red (upper) curve – $r_c/R_c = 1/9$ (central parts of the channel), the green curve – $r_c/R_c = 3/9$, the blue curve – $r_c/R_c = 7/9$, the purple curve – $r_c/R_c = 9/9$ (the edge of the channel). Accretion rate is $\dot{M} = 10^{16}$ g/s, and the Thomson scattering cross section is used. The distributions correspond to steady-state currents.

5.1. Hydrodynamics

In our calculations, the evolution of hydrodynamic characteristics was monitored until the steady flow of plasma in the channel was established. Figures 1 and 2 show dependences of velocity and pressure on height above the surface of a neutron star for steady-state flows. The negative sign of the velocity means that the motion is towards the surface. The values are averaged along the radial coordinate in the cylinder, which corresponds to one-dimensional modeling. It can be seen from the figures that the matter slows down near the surface, the deceleration being the stronger, the greater the accretion rate. It is caused by the radiative pressure on the accreted matter. The radiation is generated as a result of the impact of the incident plasma on the neutron-star surface. The deceleration of matter occurs on the scale of $\sim 1 - 2$ km. This is much smaller than the radius of the star, which justifies the cylindrical approximation for the accretion channel.

Velocity profiles in the channel for different distances from the axis of the cylinder are shown in Fig. 3. One can see that the plasma located at the center of the channel experiences the strongest deceleration, and the deceleration monotonously weakens towards the edges. However, this effect is not as pronounced as in the case of supercritical accretion (see,

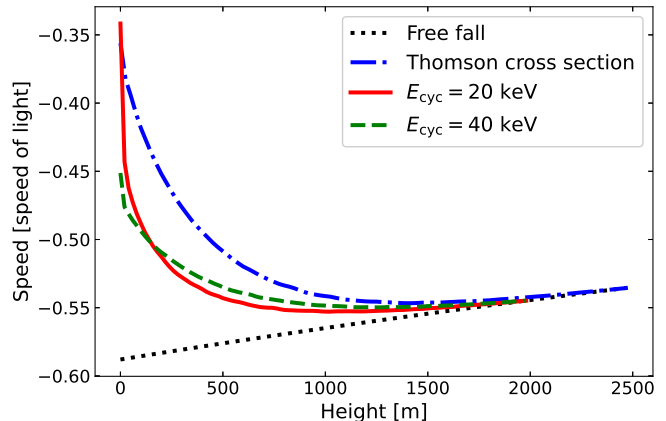


Fig. 4. Velocity profiles in units of the speed of light as functions of height above the neutron-star surface for the case of a non-magnetic Thomson cross section (blue dot-dashed line), magnetic cross section with $E_{\text{cyc}} = 20$ keV (red solid line) and $E_{\text{cyc}} = 40$ keV (green dashed line). The black dotted curve corresponds to the state of free fall. All values are averaged along the radial coordinate in the accretion channel and correspond to steady-state currents.

e.g., Mushtukov et al., 2015; Gornostaev, 2021).

In Fig. 4 we compare velocity profiles in the accretion channel obtained for the Thomson scattering cross section and the cross section in a magnetic field accounting for the cyclotron resonance. A feature of scattering in a strong magnetic field is the presence of a sharper velocity gradient in the channel areas, close to the surface of a neutron star. That is, a stronger deceleration due to resonant processes occurs at lower altitudes than in the case of Thomson scattering. Indeed, in the resonance region, the free path length a relatively small part of photons with energies $E \sim E_{\text{cyc}}$ is greatly reduced, leading to a decrease of the effective height of the deceleration. Nevertheless, at the cyclotron energy $E_{\text{cyc}} = 20$ keV ($B = 1.7 \times 10^{12}$ G) and the temperature of the boundary surface emitting the Planck spectrum $T = 3$ keV, plasma velocity v at the very neutron-star surface turns out to be approximately equal to $-0.35c$, as in the case of Thomson scattering. However, for still stronger magnetic fields, a sharp deceleration of matter at the very surface of the star is noticeably smaller than in the case of $E_{\text{cyc}} = 20$ keV. For instance, Fig. 4 shows the accretion velocity profile at $E_{\text{cyc}} = 40$ keV ($B = 3.4 \times 10^{12}$ G) and the lower boundary temperature $T = 2.8$ keV, when the velocity at the surface of the star is $v \approx -0.45c$. In this case, the energies of the majority of photons $E \sim T$ are shifted more

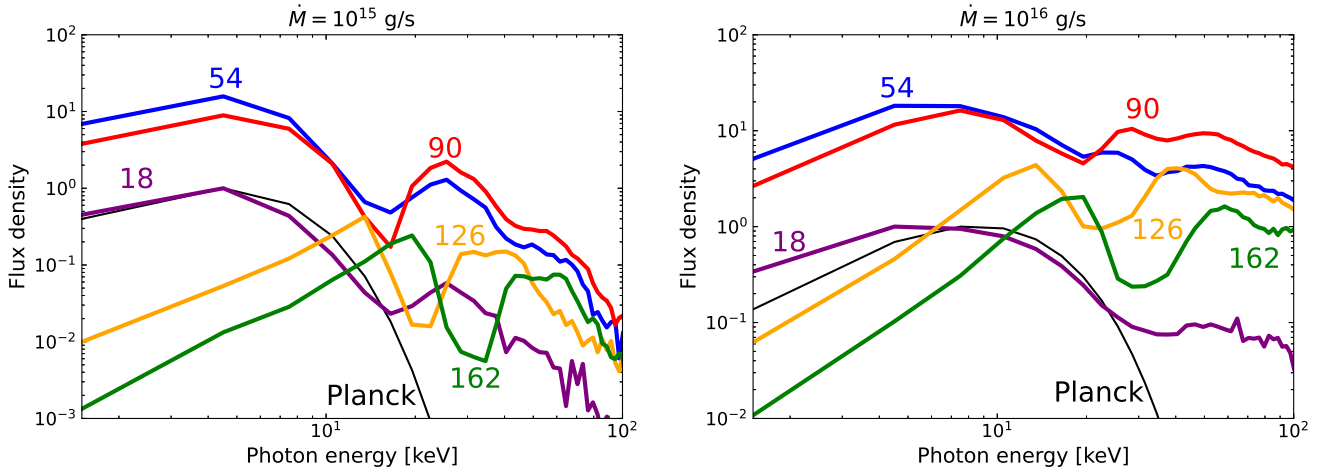


Fig. 5. The average density of the photon energy flux in the range of directions of 0.02π around the central values θ , indicated by the numbers near the curves (in degrees), as a function of the energy of photons in a magnetic field with $E_{\text{cyc}} = 20$ keV. The normalization is to the maximum of the curve with $\theta = 18^\circ$. Left panel: accretion rate $\dot{M} = 10^{15}$ g/s, right panel: $\dot{M} = 10^{16}$ g/s. Integration over the azimuthal angle has been performed.

strongly to the region of $E \ll E_{\text{cyc}}$, where scattering cross sections are suppressed by a small factor $(E/E_{\text{cyc}})^2$, while the number of resonant photons (that provide the braking) decreases significantly, which leads to a relative increase of the accreting plasma velocity.

Note that the comparison of the structure of accretion channels of subcritical pulsars with the scattering in strong magnetic fields and with the Thomson scattering agrees with the results of a similar comparison in the work of Sheng et al. (2023) for a supercritical accretion regime.

5.2. Radiation

Along with the distribution of hydrodynamic quantities, we also simulate the characteristics of radiation coming out of the accretion channel. Fig. 5 presents the spectral (over the photon energy) distributions of flux densities of the photon energy around different directions θ . Here the angle θ is measured from the outer normal to the neutron star surface, that is, the value $\theta = 90^\circ$ corresponds to the direction perpendicular to the channel walls. The cyclotron resonance corresponds to the energy $E_{\text{cyc}} = 20$ keV.

The spectra reveal cyclotron absorption lines, which are most pronounced for the angles $\theta > 90^\circ$. Photons coming out in such directions have experienced at least one scattering and are directed mainly towards the surface of the neutron star. Due to the relativistic Doppler effect the position of the cy-

clotron line depends on the angle at which the radiation exits.

Fig. 6 presents spectral fluxes in the range of angles $\theta \leq 90^\circ$. In this case, the radiation propagates directly towards the observer and does not cross the surface of the neutron star. The graphs show that the O-mode dominates at the resonance, but the X-mode starts to dominate with increasing the photon energy to $E > E_{\text{cyc}}$.

With a known radiation intensity in the two modes, one can calculate the degrees of linear (P_L) and circular (P_C) polarization. In the cold plasma approximation, they have the form (Kaminker et al., 1982)

$$P_L = \frac{I_O - I_X}{I_O + I_X} \frac{|q|}{\sqrt{1 + q^2}}, \quad P_C = \frac{I_X - I_O}{I_O + I_X} \frac{\text{sign}(q)}{\sqrt{1 + q^2}}, \quad (4)$$

where I_X is the specific intensity in the X-mode, I_O in the O-mode, $q = \frac{E_{\text{cyc}} \sin^2 \theta}{E \cdot 2 \cos \theta}$, E is the photon energy, and θ is the angle between the direction of photon and the magnetic field.

The results of calculation of the degree of linear polarization for cyclotron energies of 20 and 40 keV are shown in Fig. 7. In the resonance, the radiation is strongly polarized, while the degree of polarization can be small ($\lesssim 5 - 10\%$) at lower energies. In the region of energies above the resonance, the degree of polarization depends on the accretion rate. It follows from Fig. 7 that the degree of polarization of radiation in a fixed interval of relatively low energies $E_1 \leq E \leq E_2 < E_{\text{cyc}}$ depends on the cyclotron

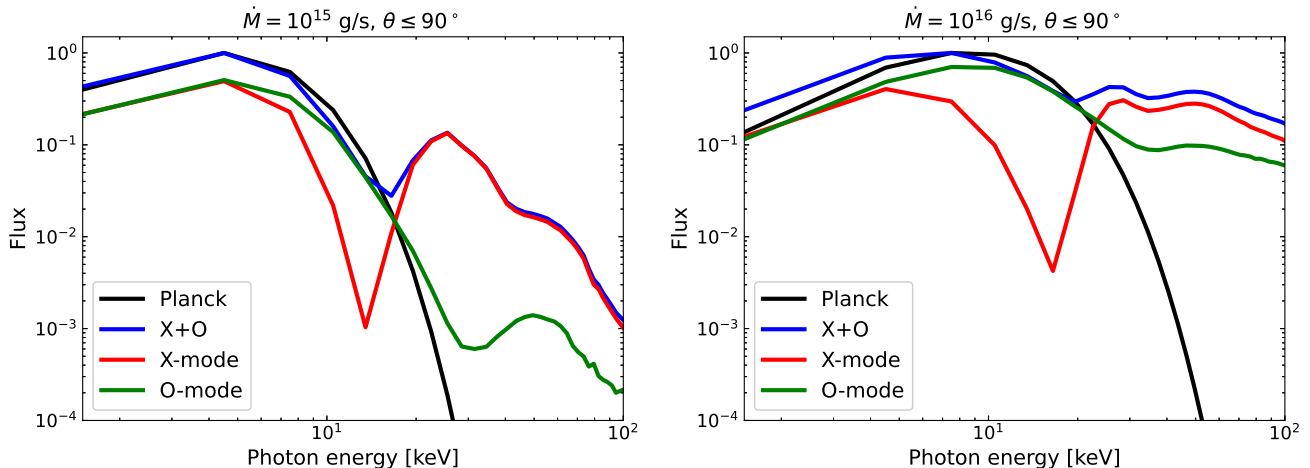


Fig. 6. Spectral fluxes coming out of the accretion channel, as functions of the photon energy for radiation in the X-mode (red curve), O-mode (green curve), and the sum of X+O modes (blue curve). The black curve corresponds to the Planck spectrum. The radiation is integrated over angles $\theta \leq 90^\circ$, normalization is to the maximum of the sum of the two modes.

resonance energy: the larger E_{cyc} , the smaller the degree of polarization. Since only a small fraction of the radiation is subject to scattering at low energies, the low degree of polarization before the resonance is a consequence of the assumption that the radiation from the lower boundary is unpolarized. However, this assumption is only the first crude approximation, and the calculation of polarization with more reliable models of boundary radiation is the subject of further research.

6. CONCLUSION

A code has been created for self-consistent calculation of the radiation hydrodynamics of matter flowing along magnetic field lines in the accretion channel of a subcritical X-ray pulsar and radiation going out of the channel, taking into account multiple scattering in a strong magnetic field. The structure of the plasma flow is modeled taking into account the resonant scattering of photons on electrons, which depends on the state of polarization of the photons. It is shown that characteristic heights of deceleration of the accretion flow above the neutron-star surface become smaller if one takes into account the influence of the magnetic field on the scattering process. We note that the total deceleration in a sufficiently strong magnetic field can be smaller than in the case of Thomson scattering.

The characteristics of radiation going from the accretion channel are calculated. Spectra of this radiation reveal cyclotron features, whose shape and

position depend on the photon propagation direction. The strongest cyclotron lines occur in the radiation that propagates towards the neutron-star surface. Therefore, when constructing a complete model of X-ray pulsar radiation, it is necessary to take into account the reflection of the channel radiation by the star's atmosphere (Poutanen et al., 2013; Kylafis et al., 2021). A detailed calculation of the radiative transfer for the two modes allows one to obtain the polarization of X-ray radiation. As a result of the simulation, it is found that radiation is strongly polarized at energies close to the resonance: the linear polarization degree is 30–40%. At low energies, polarization degree can be small ($\lesssim 5 - 10\%$), however this is a consequence of the chosen boundary conditions, rather than features of radiative transfer in the accretion channel.

At energies above the resonance, the polarization degree significantly depends on the accretion rate. If this result will be confirmed in more detailed calculations, then the degree of polarization at energies $E > E_{\text{cyc}}$ can be used as an additional parameter for determination of the accretion rate of the X-ray pulsars.

In this paper we did not take into account a number of factors that may have a significant impact on the obtained results. Despite the characteristic velocities of matter can reach half the speed of light, the approximation of non-relativistic hydrodynamics was used. In addition, the bremsstrahlung processes of absorption and emission, the influence of the magnetic field on the spectrum and polarization

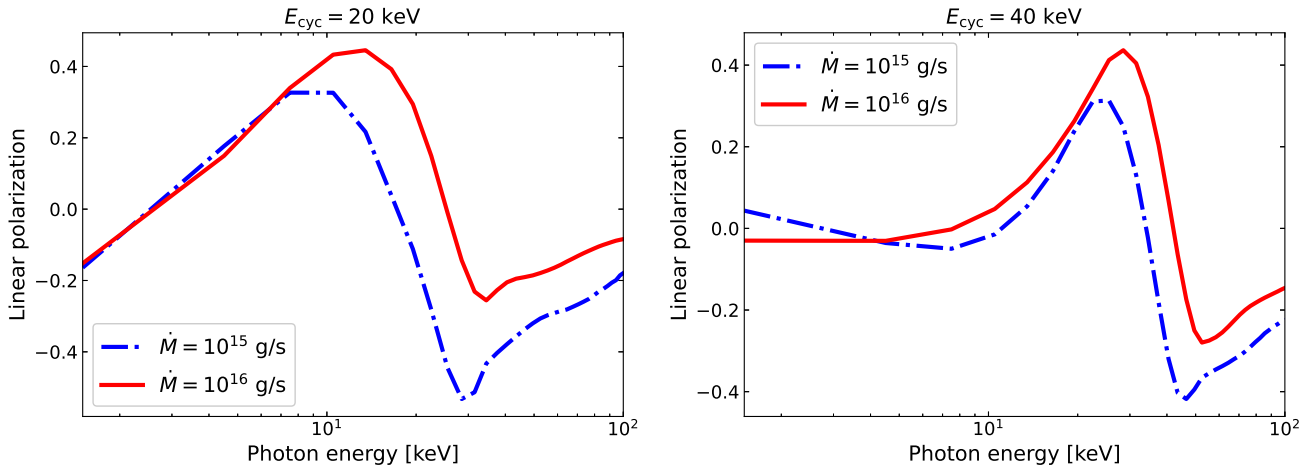


Fig. 7. The degree of linear polarization as a function of photon energy for radiation propagating in the range of angles $0 \leq \theta \leq 90^\circ$. Left: $E_{\text{cyc}} = 20$ keV, right: $E_{\text{cyc}} = 40$ keV. The blue dot-dashed line corresponds to the accretion rate $\dot{M} = 10^{15}$ g/s, and the red solid line corresponds to $\dot{M} = 10^{16}$ g/s.

of radiation coming from the surface of the star, and the effects of vacuum polarization were not taken into account. We are planning to include all these effects sequentially in future calculations.

The work of I.D.M. was supported by a grant of the Theoretical Physics and Mathematics Advancement Foundation “BASIS”.

REFERENCES

- P.K. Abolmasov and G.V. Lipunova, *MNRAS* **524**, 4148 (2023) [arXiv:2207.12312].
- M.M. Basko and R.A. Sunyaev, *MNRAS* **175**, 395 (1976).
- J.I. Castor, *Radiation Hydrodynamics* (Cambridge, UK: Cambridge University Press, 2004), p. 85.
- P. Colella and P.R. Woodward, *J. Computational Phys.* **54**, 174 (1984).
- K. Davidson, *Nature Physical Science*, **246**, 1 (1973).
- V.L. Ginzburg, *The Propagation of Electromagnetic Waves in Plasmas* (London: Pergamon, 1970).
- Yu.N. Gnedin and G.G. Pavlov, *Sov. Phys. JETP* **38**, 903 (1974).
- Yu.N. Gnedin and R.A. Sunyaev, *Astron. Astrophys.* **36**, 379 (1974).
- M.I. Gornostaev, *MNRAS* **501**, 564 (2021) [arXiv:2012.10501].
- H. Herold, *Phys. Rev. D* **19**, 2868 (1979).
- A.D. Kaminker, G.G. Pavlov, and Yu.A. Shibano, *Astrophys. Space Sci.* **86**, 249 (1982).
- J.G. Kirk, *Proc. Astron. Soc. Australia* **5**, 446 (1984).
- R.I. Klein and J. Arons, *Proceed. 23rd ESLAB Symposium on Two Topics in X-Ray Astronomy* (Ed. J. Hunt and B. Battrick; Noordwijk: ESA Publications Division, 1989), p. 89.
- N.D. Kylafis, J.E. Trümper, and N.A. Loudas, *Astron. Astrophys.* **655**, A39 (2021) [arXiv:2108.07573].
- P. Mészáros, *High-Energy Radiation from Magnetized Neutron Stars* (Chicago: Univ. of Chicago Press, 1992).
- A. Mushtukov and S. Tsygankov, *Handbook of X-ray and Gamma-ray Astrophysics*, ed. C. Bambi and A. Santangelo (Singapore: Springer, 2023), in press [arXiv:2204.14185].
- A.A. Mushtukov, V.F. Suleimanov, S.S. Tsygankov, and J. Poutanen, *MNRAS* **454**, 2539 (2015) [arXiv:1506.03600].
- A.A. Mushtukov, I.D. Markozov, V.F. Suleimanov, D.I. Nagirner, A.D. Kaminker, A.Y. Potekhin, and S. Portegies Zwart, *Phys. Rev. D* **105**, 103027 (2022) [arXiv:2204.12271].
- G.G. Pavlov and Yu.N. Gnedin, *Sov. Sci. Rev. E: Astrophys. Space Phys.* **3**, 197 (1984).
- A.Y. Potekhin and D. Lai, *MNRAS* **376**, 793 (2007) [arXiv:astro-ph/0701285].
- J. Poutanen, A.A. Mushtukov, V.F. Suleimanov, S.S. Tsygankov, D.I. Nagirner, V. Doroshenko, and A.A. Lutovinov, *Astrophys. J.* **777**, 115 (2013) [arXiv:1304.2633].
- F.-W. Schwarm, R. Ballhausen, S. Falkner, G. Schönherr, K. Pottschmidt, M.T. Wolff, P.A. Becker, F. Fürst et al., *Astron. Astrophys.* **601**, A99 (2017) [arXiv:1701.07669].
- X. Sheng, L. Zhang, O. Blaes, and Y.-F. Jiang, *MNRAS* **524**, 2431 (2023) [arXiv:2307.02410].
- V.V. Sobolev, *Course in Theoretical Astrophysics*, NASA technical translation TT F-531 (Washington, D.C.: NASA, 1969).
- A.A. Sokolov and I.M. Ternov, *Radiation from Relativistic Electrons* (New York: Am. Inst. Phys., 1986).
- B.F. West, K.D. Wolfram, and P.A. Becker, *Astrophys. J.* **835**, 129 (2017a) [arXiv:1612.02411].
- B.F. West, K.D. Wolfram, and P.A. Becker, *Astrophys. J.* **835**, 130 (2017b) [arXiv:1612.01935].